Contents

Chapter 2

Summary of Physics Reach and Comparisons With Other Experiments

The results quoted here are based on the tools described and studies reported in Part III, "Physics Simulations" of the May, 2000 BTeV proposal. (In most case these studies use GEANT3.)

All physics sensitivities and yields quoted here are explicitly for the one-arm version of BTeV. The naive expectation is that the yearly rates would be half of those quoted in the proposal. There are improvements, however, that we have taken advantage of both in hardware and our understanding of the detector that we include that increase our sensitivities. Our lepton identification procedures have been significantly improved by including the RICH detector: a full description of the gains expected are given in section 2.9. We also have investigated flavor tagging much more extensively. In our May 2000 proposal, we used an effective tagging efficiency ϵD^2 of 10% for both B^o and B_s final states, based on a preliminary study. New studies summarized in section 2.10, show that we can indeed achieve ϵD^2 of 10% for B^o decays. This more thorough study shows, as expected, that B_s decays have higher tagging efficiency because of the charged kaon produced to conserve flavor in the b quark fragmentation to a B_s. This "same side" tagging is quite favorable and, as a result, we achieve 13% for ϵD^2 in B_s decays.

Our final improvement results from an increase in our effective trigger and data acquisition bandwidth by a factor of 2.5, due to the fact that we have only one arm and schedule delays will lead to lower costs for the computing equipment used in the trigger. We decided to keep the full bandwidth of the two-arm system in our one arm plan. One reason was to keep the capability to eventually go to two arms and another was that we would have realized only a small ($\sim$10%) savings in the trigger and DAQ cost. Our original plan was to trigger on 1% of the interactions in the Level 1 trigger in the two-arm configuration. We now plan accept 2.5% of the interactions pointing into the instrumented arm by loosening the restrictions on the trigger and thereby increasing its efficiency. Simulations show that we

achieve a 15% gain in the Level 1 trigger efficiencies over those quoted in the proposal, only slightly dependent on decay mode. Fig. 2.1 shows the improvement in the Level 1 acceptance for a typical mode, $\overline{B}^o \to D^{*+}\pi^-$, where $D^{*+} \to \pi^+ D^o$, $D^o \to K^-\pi^+$.

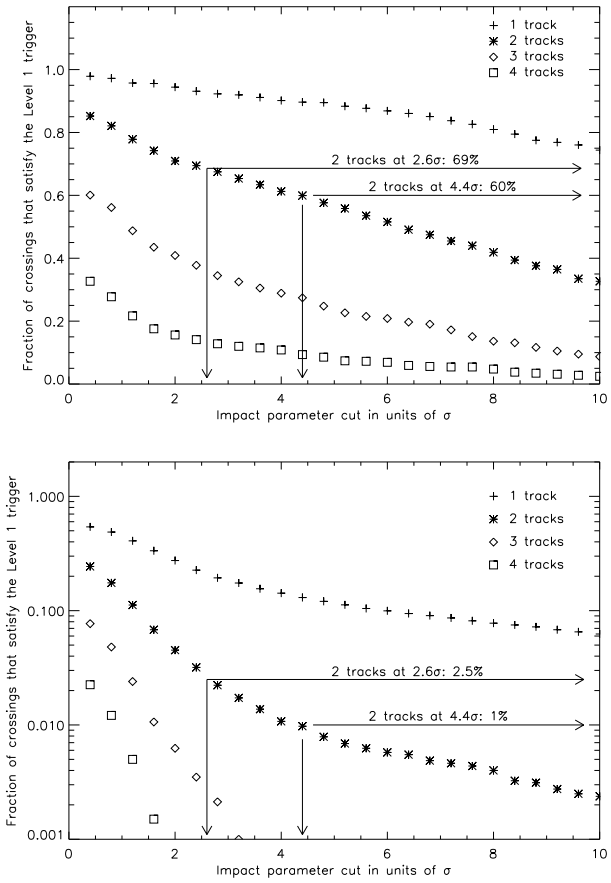

Figure 2.1: a) Trigger efficiencies for $\overline{B}^o \to D^{*+}\pi-$, $D^{*+} \to \pi^+ D^o$, $D^o \to K^-\pi^+$ for various detachment requirments in terms of normalized impact parameter (σ) and the number of detached tracks. b) Trigger response for minimum bias crossing. The arrows indicate two specific requirments, one for 2 tracks at 4.4 σ that shows a 99% rejection of minimum bias crossings (at two interactions per crossing) and 60% trigger efficiency, and other selection being 2 tracks at 2.6 σ that shows a 97.5% rejection and 69% efficiency.

2.1 Sensitivities to CP Violating Angles

BTeV will have outstanding performance in determining CP violating asymmetries. The results of our simulations are summarized in Table 2.1 for a luminosity of 2×10^{32} cm^{-2}s^{-1} and 10^7 seconds of running time.

We briefly discuss each of these measurements:

Table 2.1: Yearly sensitivities for CP violating quantities.

Quantity	Decay Mode(s)	Sensitivity
$\sin(2\beta)$	$B^o \to J/\psi K_S$	± 0.017
α	$B^o \to \rho\pi$	$\sim \pm 4.0^\circ$
γ	$B_s \to D_s^\pm K^\mp$	$\sim \pm 11.5^\circ$
γ	$B^- \to \overline{D}^o K^-$	$< \pm 13^\circ$
γ	$B \to K\pi$	$< \pm 4^\circ$ (plus theoretical errors)
$\sin(2\chi)$	$B_s \to J/\psi\eta^{(\prime)}$	± 0.024
Asymmetry	$B^o \to \pi^+\pi^-$	± 0.033

- $\sin(2\beta)$ is obtained by fitting the time distribution, which results in a 20% improvement in the error relative to that of the time-integrated asymmetry measurement.

- We use the method originally proposed by Snyder and Quinn to determine α using $B^o \to \rho\pi \to \pi^+\pi^-\pi^o$ [1]. We expect to have $\sim$500 effective flavor tagged $\rho^\pm\pi^\mp$ events and $\sim$75 $\rho^o\pi^o$ per year (10^7 s). The signal/background levels are 4.1 and 0.3, respectively. Both the signal efficiences and the background levels were determined by a full GEANT simulation. We have made a study to estimate the error in α described in more detail in Section 2.1.1, and predict an error between 1.8° and 6.1°.

  Quinn and Silva have proposed using non-flavor-tagged rates as input to improve the accuracy of the α determination [2]. We have not yet incorporated this idea.

- Although the $B \to K\pi$ modes provide the smallest experimental error in determining γ, there are model dependent errors associated with this method. On the other hand, two other methods, which use $B_s \to D_s^\pm K^\mp$ and $B^- \to \overline{D}^o K^-$, provide model independent results and can be averaged. The interplay of the three methods can be used to resolve ambiguities.

- The error in $\sin(2\chi)$ averaged over both $J/\psi\eta$ and $J/\psi\eta'$ decay modes of the B_s is $\pm 2.4\%$. Since this is approximately the value we expect, it will take us a few years to make this important measurement, if it is in the Standard Model range. Including $B_s \to J/\psi\phi$ will reduce the time.

- The asymmetry in $B^o \to \pi^+\pi^-$ may be useful to gain insight into the value of α with theoretical input or combined with $B_s \to K^+K^-$ and theory to obtain γ. This study was done both with MCFast and GEANT. The signal efficiency is 10% higher in MCFast and the background levels the same in both, within statistics.

2.1.1 Sensitivity in Determining α Using $B^o \to \rho\pi$

At the time of the proposal, we used estimates from the literature to get a rough estimate the sensitivity we will have in measuring α using $B^o \to \rho\pi$. This requires the measurement of the tagged, time-dependent CP asymmetry in a particular combination of amplitudes obtained from a Dalitz plot analysis of the decay. The combination of amplitudes causes the Penguin terms to cancel and isolates the tree contribution to the decay, which provides the value of α. We have now performed a Dalitz plot analysis that includes detector resolution and background along with the expected levels of detected signal events.

The decay amplitude may be written as

$$\mid B^0\rangle = f_+ a_{+-} + f_- a_{-+} + f_0 a_{00},$$

where $a_{i,j}$ refers to the three distinct final states as

$$a_{i,j} = a(B^0 \to \rho^i \pi^j),\ (i,j) = (+,-),(-,+),(0,0),$$

and f_k parameterizes the ρ decay amplitude. We use

$$f_k(s) = \frac{\cos\theta_k}{s - m_\rho^2 + i\prod(s)},$$

where θ_k is the angle between the direction of the B and the direction of a daughter pion, both viewed in the ρ rest frame, and s is the square of the dipion invariant mass $s = (E_{\pi_1} + E_{\pi_2})^2 - (\overrightarrow{p}_{\pi_1} + \overrightarrow{p}_{\pi_2})^2$; s can be in one of three charge states, s^+, s^- or s^o. In each case

$$\prod(s) = \frac{m_\rho^2}{\sqrt{s}} \left(\frac{p(s)}{p(m_\rho^2)}\right)^3 \Gamma_\rho(m_\rho^2),$$

p being the momentum in the ρ rest frame.

The amplitudes $a_{i,j}$ for B^o and $\overline{B^o}$ decay are written as a sum of Tree (T) and Penguin (P) parts as

$$\begin{aligned}
a_{+-} &= -e^{i\gamma}T^{+-} + e^{-i\beta}P^{+-} \\
a_{-+} &= -e^{i\gamma}T^{-+} + e^{-i\beta}P^{-+} \\
a_{00} &= -e^{i\gamma}T^{00} + e^{-i\beta}P^{00} \\
\bar{a}_{+-} &= -e^{-i\gamma}T^{-+} + e^{i\beta}P^{-+} \\
\bar{a}_{-+} &= -e^{-i\gamma}T^{+-} + e^{i\beta}P^{+-} \\
\bar{a}_{00} &= -e^{-i\gamma}T^{00} + e^{i\beta}P^{00},
\end{aligned}$$

where γ and β are the usual CKM angles and $\alpha + \beta + \gamma = \pi$. Using both isospsin symmetry and the fact that the Penguin amplitude is a pure $\Delta I = 1/2$ transition leads to the replacement

$$P^{00} = -\frac{1}{2}(P^{+-} + P^{-+}).$$

This leaves us with 9 parameters to be fit to the data including α, 3 complex Tree and 2 Penguin amplitudes, where one is defined as purely real and the total rate is used as an independent input. We can also allow the resonant and non-resonant background fractions to be determined by the fit, which adds two additional parameters.

Signal events are generated using the averaged branching ratio for $B^o \to \rho^+\pi^-$ and $B^o \to \rho^-\pi^+$ of 2.8×10^{-5} and a rate of 0.5×10^{-5} for $\rho^o\pi^o$. For this study we generated a data sample corresponding to two years of running (2×10^7s) with the one-arm version of BTeV. The background level is determined by a full GEANT simulation of 4,450,000 generic $b\overline{b}$ events; it is assumed that this background has an exponential time dependence given by the average lifetime of b-flavored hadrons. The background is parameterized with both resonant and non-resonant components. The non-resonant background is distributed uniformly over the Dalitz plot. The resonant background allows for two of the pions to have a Breit-Wigner shaped low mass enhancement. All charged tracks and photons in both signal and background events are smeared by the detector resolution before further analysis. Signal events are generated with an exponential time distribution modified by B^o mixing. The simulation is repeated for different assumptions about the relative size of Penguin and Tree amplitudes and the fraction of resonant and non-resonant background. For each set of data a maximum likelihood fit is performed where the likelihood is given by

$$-2\ln\mathcal{L} = -2\sum_{i=1}^{N_{B^o}} \ln\Bigg[\Bigg(\frac{\mid \mathcal{A}(s_i^+, s_i^-, t_i; \alpha, ..) \mid^2}{\mathcal{N}(\alpha, ..)} \times \varepsilon(s_i^+, s_i^-) + R_{non} \times \frac{1}{\mathcal{N}_t} + R_{res} \times \frac{\mid \mathcal{BW}(s_i^+, s_i^-) \mid^2}{\mathcal{N}_{BW}} \times \varepsilon(s_i^+, s_i^-)\Bigg)/(1 + R_{non} + R_{res})\Bigg]$$

$$-2\sum_{j=1}^{N_{\overline{B}^o}} \ln\Bigg[\Bigg(\frac{\mid \bar{\mathcal{A}}(s_j^+, s_j^-, t_j; \alpha, ..) \mid^2}{\mathcal{N}(\alpha, ..)} \times \varepsilon(s_i^+, s_i^-) + R_{non} \times \frac{1}{\mathcal{N}_t} + R_{res} \times \frac{\mid \mathcal{BW}(s_j^+, s_j^-) \mid^2}{\mathcal{N}_{BW}} \times \varepsilon(s_j^+, s_j^-)\Bigg)/(1 + R_{non} + R_{res})\Bigg],$$

where N_{B^o} and $N_{\overline{B}^o}$ are the total number of B^o and $\overline{B}^o$ events, respectively, and $\mathcal{N}$ is the normalization. It is given by $(\mid \mathcal{A} \mid^2 + \mid \bar{\mathcal{A}} \mid^2) \times \varepsilon$, integrated over the Dalitz plot acceptance, where ε is the detector efficiency. R_{non} and R_{res} are the ratios of non-resonant and resonant background to signal. For one case we show in Fig. 2.2 the χ^2 contours for α and correlations with the fractions of resonant and non-resonant backgrounds. The input value for α in this case was 77.3°. The fit has no trouble picking out the correct solution.

Table 2.2 shows the results of an ensemble of fits with different assumptions on the fractions of resonant and non-resonant background, and different values of α. The one parameter fit assumes that the non-resonant and resonant background levels are determined from non-flavor tagged data, while in the three parameter fit, these are determined along with α.

These studies show that over a broad range of background models, α is determined with a sensitivity between 1.4°-4.3° in 2×10^7s of running time. The sensitivity will also depend

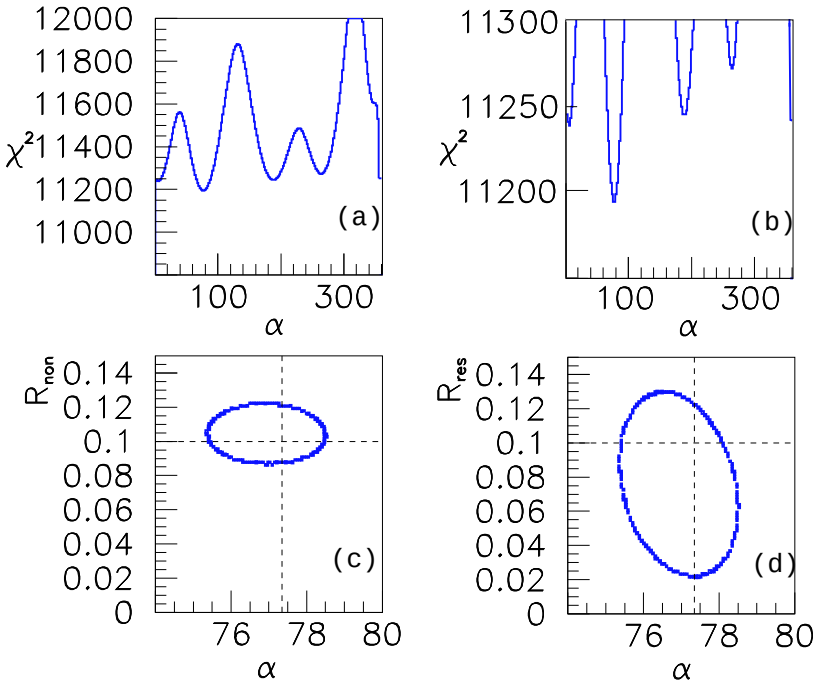

Figure 2.2: Results of a simulation using 1000 $B^o \to \rho\pi$ detected signal events with an input value of $\alpha = 77.3°$. (a) The χ^2 contours as a function of α. (b) same as (a) with the vertical scale enlarged. (c) The correlation of the best fit for α and R_{non} and (d) The correlation of the best fit for α and R_{res}.

on several unknown quantities including the branching ratio for $\rho^o\pi^o$, and the ratio of Tree to Penguin amplitudes.

2.2 Sensitivity to B_s Mixing

BTeV can definitively reach x_s values of 75 in 2×10^7 seconds of running. Put another way, it will take us only 10 days of steady running to reach x_s of 20. These estimates are based on the decay mode $B_s \to D_s^+\pi^-$, with $D_s^+ \to \phi\pi^+$ and $K^{*o}K^+$. "Definitively" is used here to express the ability to make a measurement where the best solution for a fit to the oscillation frequency is better by "5 standard deviations" than the next best fit. Thus BTeV can cover the entire range of x_s values allowed in the Standard Model.

2.3 Reach in Rare Decays

BTeV has excellent reach in rare decays. We have investigated the exclusive decays $B^o \to K^{*o}\mu^+\mu^-$, $B^+ \to K^+\mu^+\mu^-$ and the inclusive decay $B \to X_s\mu^+\mu^-$.

Table 2.2: Results of Determining α with 1000 $B^o \to \rho\pi$ Events.

α	Background, %		$\langle\alpha\rangle$	$\langle\sigma_\alpha\rangle$	$\langle\alpha\rangle$	$\langle\sigma_\alpha\rangle$
MC	Resonant.	Nonres.	1 parameter		3 parameters	
77.3	0	0	77.4	1.3	77.3	1.4
	10	10	77.4	1.4	77.3	1.5
	20	20	77.2	1.5	77.2	1.6
	40	0	77.4	1.6	77.2	1.8
	0	40	77.6	1.4	77.1	1.6
93.0	0	0	92.7	1.4	92.8	1.5
	10	10	93.3	1.6	93.4	1.8
	20	20	93.1	1.7	93.3	1.9
	40	0	92.7	1.8	93.2	2.1
	0	40	92.5	1.6	93.3	1.9
111.0	0	0	111.0	1.9	111.7	2.3
	10	10	110.7	2.3	110.6	3.6
	20	20	110.9	2.7	111.7	3.9
	40	0	111.2	2.8	110.4	4.3
	0	40	110.2	2.1	111.1	4.0

We acquire $\sim$2530 $K^{*o}\mu^+\mu^-$ decays in 10^7 seconds, enough to measure the lepton-forward-backward asymmetry and test the Standard Model. Although the asymmetry is expected to be small in $K^+\mu^+\mu^-$, we test the Standard Model expectation, due to our large sample of $\sim$1300 events per year.

We also expect to be able to measure the inclusive rate $b \to s\mu^+\mu^+$ with 20σ significance. This inclusive rate is very important. It could either show non-Standard Model physics or greatly constrain alternative models.

2.4 Sensitivities in New Physics Modes

Precision studies of b decays can bring a wealth of information to bear on new physics, that probably will be crucial in sorting out anything seen at the LHC (see Chapter 1). The BTeV data samples will be large enough to test different scenarios emerging from "New Physics" at the TeV energy scale. In Table 2.3 we show the expected rates in BTeV for one year of running (10^7 s) and an e^+e^- B-factory operating at the $\Upsilon(4S)$ with a total accumulated sample of 500 fb^{-1}, about what is expected before BTeV begins running. More comparisons with e^+e^- are given in the next section.

Table 2.3: Comparison of BTeV and B-factory Yields on Different Time Scales.

Mode	BTeV ($10^7 s$)			B-factory (500 fb^{-1})		
	Yield	Tagged†	S/B	Yield	Tagged†	S/B
$B_s \to J/\psi\eta^{(\prime)}$	12650	1645	>15			
$B^- \to \phi K^-$	6325	6325	>10	700	700	4
$B^o \to \phi K_s$	1150	115	5.2	250	75	4
$B^o \to K^{*o}\mu^+\mu^-$	2530	2530	11	∼50	∼50	3 [3]
$B_s \to \mu^+\mu^-$	6	0.7	> 15	0		
$B_d \to \mu^+\mu^-$	1	0.1	> 10	0		
$D^{*+} \to \pi^+ D^o$; $D^o \to K^-\pi^+$	$\sim 10^8$	$\sim 10^8$	large	8×10^5	8×10^5	large

$\dagger$ Tagged here means that the initial flavor of the B is determined.

2.5 Comparison with e^+e^- B Factories

Much of what is known about b decays has been learned at e^+e^- machines [4]. Machines operating at the $\Upsilon(4S)$ found the first fully reconstructed B mesons (CLEO), B^o-$\overline{B}^o$ mixing (ARGUS), the first signal for the $b \to u$ transition (CLEO), and Penguin decays (CLEO). Lifetimes of b hadrons were first measured by experiments at PEP, slightly later at PETRA, and extended and improved by LEP [4].

The success of the $\Upsilon(4S)$ machines, CESR and DORIS, led to the construction at KEK and SLAC of two new $\Upsilon(4S)$ machines with luminosity goals in excess of $3 \times 10^{33}\text{cm}^{-2}\text{s}^{-1}$. These machines have asymmetric beam energies so they can measure time dependent CP violation. In fact, CP violation in B_d was convincingly demonstrated recently by both the BABAR and BELLE experiments [5]. These machines, however, will investigate only B^o and $B^\pm$ decays. They will not investigate B_s, B_c or Λ_b decays. While, in principle, the e^+e^- machines could run on the $\Upsilon(5S)$, which is likely to be a source of B_s mesons, there are crucial concerns that vitiate any such approach: The predicted cross-section for B_s production is only ∼0.1 of that of B production on the $\Upsilon(4S)$. Furthermore the proper time resolution necessary to resolve B_s oscillations cannot be obtained using the relatively slow B_s mesons produced at the $\Upsilon(5S)$

Table 2.4 shows a comparison between BTeV and an asymmetric e^+e^- machine for measuring the CP violating asymmetry in the decay mode $B^o \to \pi^+\pi^-$. The peak luminosity for the e^+e^- machines is set at 10^{34} cm^{-2}s^{-1}, a value higher that what has been achieved. The detection and tagging efficiencies are taken from Aubert *et al* [6]. For the B^o branching fraction we use the world average values computed in the "Physics Case" part of this document. In Table 2.5 we show a similar comparison for the final state $B^- \to \overline{D}^o K^-$, a mode that could be used to determine the CKM angle γ. It is clear that the large hadronic b production cross section can overwhelm the much smaller e^+e^- rate. Furthermore, the e^+e^- B factories do not have access to the important CP violation measurements that need to be made in B_s decays. (See Table 2.3 for more comparisons.)

Table 2.4: Number of tagged $B^o \to \pi^+\pi^-$ ($\mathcal{B}$=0.45 $\times$ 10^{-5}).

	$\mathcal{L}$(cm^{-2}s^{-1})	σ	# $B^o/10^7$ s	Signal Efficiency	Tagging ϵD^2	# tagged/10^7 s
e^+e^-	10^{34}	1.1 nb	1.1×10^8	0.45	0.26	56
BTeV	2×10^{32}	100μb	1.5×10^{11}	0.021	0.1	1426

Table 2.5: Number of $B^- \to \overline{D}^o K^-$ ($\mathcal{B}$=1.7 $\times$ 10^{-7}).

	$\mathcal{L}$(cm^{-2}s^{-1})	σ	# $B^-/10^7$ s	Signal Efficiency	Events/10^7 s
e^+e^-	10^{34}	1.1 nb	1.1×10^8	0.4	5
BTeV	2×10^{32}	100μb	1.5×10^{11}	0.007	176

2.5.1 Comments on Upgrades to KEK-B and PEP-II

In 2001 PEP-II and KEK-B delivered 40 fb^{-1} and 36 fb^{-1}, respectively. This corresponds to about 4×10^7 B^o mesons and 4×10^7 $B^\mp$ mesons produced for each experiment. The peak luminosities for both machines are about 5×10^{33}cm^{-2}s^{-1}.

KEK-B is planning on how to upgrade to a luminosity of 10^{35}cm^{-2}s^{-1}, ten times their original design using the same machine configuration, with a target date of 2007. (Much of the reference material in this section comes from the E2 Snowmass working group report [7].) However, as pointed out in the E2 report, the higher luminosity can cause problems for the detector: "Operation at 10^{35} has implications for the detector and the IR. The rates from collisions will be significantly higher which will lead to larger occupancy. Trigger rates and rates through the data acquisition system will be higher. There will be more synchrotron radiation, which will have to be removed by masking. There may be larger vacuum pressure resulting in higher background rates from Touschek scattering. There may need to be a larger crossing angle which may make it harder to shield backgrounds efficiently. The final quads may be moved closer to the IP to reduce β^*. And finally, the background at injection might be significantly worse...the first few layers of the silicon vertex detector will have high occupancy and will be replaced by pixel detectors. Beampipe heating due especially to Higher Order Modes (HOM) requires that the beam pipe be water cooled. The Central Drift Chamber is undergoing a modification in 2002 to replace the two inner layers with a small cell chamber. It is expected to be able to handle super-KEK rates. The CsI(Tl) calorimeter is slow and something may need to be done to it. The RPCs in the muon system already suffer from inefficiency due to local deadtime and will probably need to be replaced with wire chambers. The data acquisition system will also have to be upgraded."

The Super-BABAR concept requires a new machine operating in either the PEP tunnel

or the SLC arcs that achieves a luminosity of $10^{36}\mathrm{cm}^{-2}\mathrm{s}^{-1}$. According to the E2 Snowmass summary: "The goal is to be competitive with the next generation hadron collider experiments, at least in the area of B_d and B_u physics." However, in order to reach this goal, the machine must be successfully built and the detector essentially completely rebuilt to withstand the high rates and radiation load. The challenges for both the detector and the accelerator are enormous. Stu Henderson in his Snowmass summary talk said about machine: "Every parameter is pushed to the limit-many accelerator physics and technology issues [8]."

Concerning the detector, the E2 summary states: "Most of the BABAR subsystems will have to undergo some modification or replacement to handle the much higher rates of the new machine. To carry out the program, the overall performance, in terms of resolution, efficiency, and background rejection, must be similar to that of BABAR. The detector must retain its high degree of hermeticity as well.

"There are many questions about the cost and availability of suitable detector technologies which will need to be studied before the detector design can be finalized. We give four examples. (1) To maintain the vertex resolution of BABAR and withstand the radiation environment, pixels with a material budget of 0.3% X_o per layer are proposed. Traditional pixel detectors which consist of a silicon pixel array bump-bonded to a readout chip are at least 1.0% X_o. To obtain less material, monolithic pixel detectors are suggested. This technology has never been used in a particle physics experiment. (2) As a drift chamber cannot cope with the large rates and large accumulated charge, a silicon microstrip tracker has been proposed. At these low energies track parameter resolution is dominated by multiple Coulomb scattering. Silicon microstrip technology is well tested but is usually used at this energy for vertexing, not tracking. Realistic simulations need to be performed to establish if momentum resolution as good as BABAR can be achieved with the large amount of material present in the silicon tracker. If not, we suggest a TPC, possibly readout with a Gas Electron Multiplier, or MICROMEGAS, be explored as an alternative to the silicon tracker (3) There is no established crystal technology to replace the CsI(Tl). There are some candidate materials but the most attractive have not been used in a calorimeter previously. (4) There is no known technology for the light sensor for the SuperDIRC.

"Since the goal of the SuperKEK and SuperBABAR upgrades are to enable the e^+e^- machine to compete with future hadron collider experiments, it is important to make a realistic evaluation of the sensitivities of all these experiments over a wide range of final states. Such projections are, of course, somewhat uncertain. The sensitivities of future hadron collider experiments have been determined from detailed and sophisticated simulations of signals and backgrounds. As these simulations are an approximation to reality, the performance of LHCb and BTeV may be somewhat better or somewhat worse than the simulations predict. Projections for SuperBABAR are, at this point, mainly done by scaling from BABAR experience assuming that the new detector, which still has many open R&D issues, will achieve the same efficiency that BABAR now achieves even though the luminosity will be a factor of 300 higher. More realistic studies need to be performed before a full comparison between SuperBABAR and the hadron collider experiments is made. With these caveats a compari-

Table 2.6: Comparison of CP Reach of Hadron Collider Experiments and SuperBABAR. The last column is a prediction of which kind of facility will make the dominant contribution to each physics measurement. (From the E2 summary [7].)

	BTeV† 10^7s	LHCb 10^7s	BABAR Belle (2005)	e^+e^- 10^{35} 10^7s	e^+e^- 10^{36} 10^7s	e^+e^- at 10^{36} vs hadron collider
$\sin 2\beta$	0.017	0.02	0.037	0.026	0.008	Equal
$\sin 2\alpha$	0.05	0.05	0.14	0.1	0.032	Equal
$\gamma\,[B_s(D_sK)]$	$\sim 11.5^o$					Had
$\gamma\,[B(DK)]$	$\sim 13.2^o$		$\sim 20^o$		12^o	Equal
$\sin 2\chi$	0.024	0.04	-	-	-	Had
$\mathcal{B}(B \to \pi^o\pi^o)$	-	-	$\sim$20%	14 %	6%	e^+e^-
V_{ub}	-	-	$\sim$2.3%	$\sim$1% (sys)	$\sim$1% (sys)	e^+e^-

† We have changed the BTeV numbers to correspond to the one-arm version.

son of BTeV, LHCb, BABAR and Belle in 2005, and the e^+e^- machines at 10^{35} and 10^{36} is given in Table 2.6 for several states of importance to the study of *CP* violation in B decays."

This study indeed demonstrates that it will take a $10^{36} cm^{-2} s^{-1}$ e^+e^- collider operating at the $\Upsilon(4S)$ to match the performance of BTeV on B^o and $B^{\mp}$ mesons, while there will be no competition for the B_s or other b-flavored hadrons. There are serious technical problems that both the machine and the detector would need to surmount. We believe the cost will far exceed that of BTeV. The HEPAP subpanel in their report [9] mentions a 500 M$ number for the detector. That cost has not been subject to review.

We note that the LHCb sensitivity for $\sin 2\alpha$ is quoted as 0.05, the same as BTeV even though BTeV gathers twice as many events and has a much better signal to background (see section 2.7.2). This LHCb number comes from P. Ball *et al* [10] where these caveats are included: "It should be stressed that the fitting studies are preliminary and are optimistic in the fact that the exact LHCb acceptance has not been used and the backgrounds have not been included..."

2.6 Comparison with CDF, D0, CMS, and ATLAS

Both CDF and D0 have measured the b production cross section [11]. CDF has contributed to our knowledge of b decay mostly by its measurements of the lifetime of b-flavored hadrons [12], which are competitive with those of LEP [13] and recently through its discovery of the B_c meson [14]. CDF also saw the first hint for CP violation in the b system [15]. These detectors were designed for physics discoveries at large transverse momentum. It is remarkable that they have been able to accomplish so much in b physics. They have shown that it is possible to do b physics in the environment of a hadron collider.

However, these detectors, and the new central detectors ATLAS and CMS are very far from optimal for b physics. BTeV has been designed with b physics as its primary goal. To have an efficient trigger based on separation of b decays from the primary, BTeV uses the large $|\eta|$ region where the b's are boosted. The detached vertex trigger allows collection with very high efficiency of interesting purely hadronic final states such as $\pi^+\pi^-$, $\rho\pi$, $D_s^+\pi^-$ and $D_s^+K^-$. It is also efficient on an eclectic mixture of all b decays and is therefore open to decays which may not be considered "interesting" now or at the time of data taking, but may become so as our knowledge improves. It also allows us to collect enough charm to investigate charm mixing and CP violation.

The use of the forward geometry also allows for excellent charged hadron identification over a wide momentum range, with a gaseous RICH detector. This is crucial for many physics issues such as separating $K\pi$ from $\pi\pi$, $D_s\pi$ from D_sK, kaon flavor tagging, etc.

Furthermore an experiment that plans on answering all the open questions in b physics, requires a high quality electromagnetic calorimeter. Installation of such a calorimeter in the CLEO detector made new physics vistas possible and such a device in BTeV allows for the measurement of several crucial final states such as $B^o \to \rho\pi$, and $B_s \to J/\psi\eta'$. The only central detector that is planning to have a high quality electromagnetic calorimeter is CMS.

Finally, BTeV has all the crucial elements required to study any newly suggested b or charm process or uncover new physics. The crucial elements are:

- a detached vertex algorithm in the first trigger level,
- highly efficient particle identification across the entire momentum range with good ($\approx$ 100:1) background rejection,
- an electromagnetic calorimeter with sufficiently good energy resolution and efficiency to fully reconstruct rare B decay final states with single photons or neutral pions.

BTeV will have a physics reach substantially beyond that of CDF, D0, CMS, and ATLAS. The sensitivities of CDF and D0 are summarized in Anikeev *et al* [16] and those of CMS and ATLAS in Ball *et al* [10].

2.7 Comparison with LHCb

2.7.1 General Comparisons

LHCb [17] is an experiment planned for the LHC with almost the same physics goals as BTeV. Here we show how BTeV can compete with LHCb in many areas and why it is a superior experiment in some very important areas. Both experiments intend to run at a luminosity of 2×10^{32} cm^{-2}s^{-1}. There are several inherent advantages and disadvantages that LHCb has compared with BTeV. The issues that favor LHCb are:

- The b production cross-section is expected to be about five times larger at the LHC than at the Tevatron, while the total cross-section is only 1.6 times as large.

- The mean number of interactions per bunch crossing is expected to be about 3 times lower at the LHC than at the Tevatron.

The issues that favor BTeV are:

- The seven times larger beam energy at the LHC makes the momentum range of particles that need to be tracked and identified much larger and therefore more difficult. The larger energy also causes a large increase in track multiplicity per event, which makes pattern recognition and triggering more difficult.

- The interaction region at the Tevatron is three to six times longer along the beam direction than at LHC ($\sigma_z = 5$ cm), which allows BTeV to be able to accept collisions with a mean of two interactions per crossing, since the interactions are well separated in z. LHCb plans to veto crossings with more than one interaction.

- The short bunch spacing at the LHC, 25 ns, has serious negative effects on all their detector subsystems. There are occupancy problems if the sub-detector integration times are long. This can be avoided by having short integration times, but that markedly increases the electronics noise. For example, in a silicon detector these considerations make first level detached vertex triggering more difficult than at the Tevatron; BTeV has a more relaxed 132 ns bunch spacing, 5.3 times longer. In fact, the current plan of LHCb is to trigger in their first trigger level on muons, electrons or hadrons of moderate p_t, and detect detached vertices in the next trigger level.

- BTeV is designed to have the vertex detector in the magnetic field, thus allowing the rejection of low momentum tracks at the trigger level. Low momentum tracks are more susceptible to multiple scattering which can cause false detached vertices leading to poor background rejection in the trigger.

- BTeV is designed with a high quality $PbWO_4$ electromagnetic calorimeter, that provides high resolution and acceptance for interesting final states with γ's, π^o's, and $\eta^{(\prime)}$'s. The BTeV electromagnetic calorimeter is superior in energy resolution and segmentation to LHCb's. LHCb has a Shaslik-style Pb-scintillating fiber device, following a preshower detector. The LHCb energy resolution is $10\%/\sqrt{E} \oplus 1.5\%$, which compares poorly with BTeV's $1.7\%/\sqrt{E} \oplus 0.55\%$. The LHCb detector segmentation is 4 cm $\times$ 4 cm up to $\sim$90 mr, 8 cm $\times$ 8 cm to $\sim$160 mr and 16 cm $\times$ 16 cm at larger angles. (The distance to the interaction point is 12.4 m.) Thus the segmentation is comparable to BTeV only in the inner region. (BTeV has 2.8 cm $\times$ 2.8 cm crystals 7.4 m from the center of the interaction region.)

- Use of a detached vertex trigger at Level 1 allows for an extensive charm physics program absent in LHCb. It also accepts a more general collection of b events, which are less oriented towards particular final states.

- The LHCb data acquisition system is designed to output 200 Hz of b decays, while BTeV is designed for larger output bandwidth of 1,000 Hz of b's and 1,000 Hz of charm, and an additional 2000 Hz for contingency, calibration events, and other physics. Therefore, BTeV has access to a much wider range of heavy quark decays.

We have compensated for LHCb's initial advantages in b cross-section due their higher center-of-mass energy. In fact, the high energy actually works in many ways as a disadvantage. For example, LHCb needs two RICH counters to cover the momentum range in their one arm. Particle identification and other considerations force LHCb to be longer than BTeV. Its single arm is twice as long as one of BTeV arms. As a result, LHCb's transverse size is twice that of BTeV (linear dimension), in order to cover the same solid angle. It is expensive to instrument all of this real estate with high quality particle detectors. Thus, the total cost for LHCb based only on instrumented area, (a naive assumption) would be four times the total cost for BTeV.

We have done a detailed comparison between BTeV and LHCb using two modes of great importance because they give direct determinations of the CP violating angles α and γ, and report our results here.

2.7.2 A Specific Comparison: $B^o \to \rho\pi$

We base our comparison on the total number of untagged events quoted by both experiments. The BTeV numbers come from Part III of this document. The LHCb numbers are found in their Technical Design Report [17]. Both sets of numbers are calculated for 10^7 seconds at a luminosity of 2×10^{32} cm^{-2}s^{-1}. We have corrected the LHCb numbers by normalizing them to the branching ratios used by BTeV. In Table 2.7 we compare the relevant quantities [18].

Table 2.7: Event yields and signal/background for $B^o \to \rho\pi$.

Mode	Branching Ratio	BTeV		LHCb	
		Yield	S/B	Yield	S/B
$B^o \to \rho^{\pm}\pi^{\mp}$	2.8×10^{-5}	5400	4.1	2140	0.8
$B^o \to \rho^o\pi^0$	0.5×10^{-5}	776	0.3	880	-

LHCb has done a background estimate based on a heavily preselected sample of events [19]. These include:

- a preselection for charged pions and photons which required the momentum or energy to exceed a value depending on the polar angle of the candidate. For charged pions, the momentum cut varied between 1 and 2 GeV/c and for photons the energy cut varied between 2 and 6 GeV;

- selection of signal-like events based on a discriminant variable built from kinematic variables of the π, ρ and B^o;

- selection based on the reconstructed secondary vertex for a $\pi^+\pi^-$ combination; and
- Dalitz plot cuts to eliminate low energy π^o combinatorial background due to particles from the primary vertex.

These cuts are applied to the generator event sample before the events are processed through GEANT [20]. The BTeV simulation was carried out without any preselection cuts. We were worried that the preselection would bias us to lower background rates. For example, if two photons overlapped or interactions of charged tracks put energy into photon clusters these can well become part of our background sample. Thus the LHCb background estimate may well be only a lower limit.

We note that their π^o mass resolution varies between 5 and 10 MeV/c^2 (r.m.s.) and their B^o mass resolution is 50 MeV/c^2 (r.m.s.). The corresponding numbers for BTeV are 3.1 MeV/c^2 and 28 MeV/c^2.

With this analysis, LHCb claims signal/background (S/B) of 1.3 for $\rho^\pm\pi^\mp$, where they have assumed a branching ratio of 4.4×10^{-5}. For our assumed branching ratio, S/B is 0.8; The S/B for BTeV is 4.1. Furthermore, the BTeV background analysis was done without preselection and therefore is likely to be more realistic. For the final state $\rho^o\pi^o$ LHCb has not produced a background estimate; in our experience it is difficult to estimate signal efficiencies without evaluating how restrictive the selection criteria need to be to reduce backgrounds.

It is not surprising that BTeV's superior crystal calorimeter and detached vertex trigger produce a large advantage in this final state over LHCb, even using LHCb's optimistic numbers. BTeV has a factor of 2.2 advantage in signal yield in $\rho^\pm\pi^\mp$ and a better S/B by a factor of 5. This results in an advantage to BTeV in the number of "effective events" (events weighted by dilution due to background) of almost a factor of 4.

2.7.3 $B_s \to D_s^\pm K^\mp$

A comparison of the estimated total efficiencies (excluding D_s decay branching ratios), B_s mass resolutions, and S:B ratios are given in Table 2.8. Here $D_s^+ \to K^+K^-\pi^+$ can be reconstructed via either $\phi\pi^+$ or $K^{*o}K^-$. Here BTeV and LHCb differ somewhat. LHCb has the same efficiency in both modes, whereas BTeV analyzes them somewhat differently. For $K^{*o}K^-$ BTeV requires both charged kaons to hit the RICH detector, while for $\phi\pi^+$ only one charged kaon is required to be identified in the RICH. (The reconstruction efficiency for $\phi\pi^+$ is 2.3%, while for $K^{*o}K^-$ it is 1.3%).

Table 2.8: Comparison of BTeV and LHCb sensitivities for $B_s \to D_s^\pm K^\mp$.

Branching Ratio	BTeV		LHCb	
	Yield	S/B	Yield	S/B
3×10^{-4}	7,530	7	7,660	7

The yields and signal/background are about the same in this mode. This is not unexpected. The LHCb trigger efficiency is 4.1 times lower than BTeV and the acceptances are about equal. This factor of 4 should neutralize the LHCb cross-section advantage, of a factor of 5, and in this study it has.

2.8 Summary

BTeV is far superior to current e^+e^- colliders operating on the $\Upsilon(4S)$ because of the enormous difference in the b rate. For reconstructed B^+ and B^o decays, BTeV has a factor of $\sim$200 more rate. Furthermore, the important B_s physics cannot be done at the e^+e^- machines. A luminosity on the order of $10^{36}\text{cm}^{-2}\text{s}^{-1}$ would need to be achieved before these machines would be competitive in B^o and $B^\pm$ physics with BTeV.

CDF, D0, CMS, and ATLAS cannot compete in areas where particle identification or photon detection are important; as a result, the b-physics reach of BTeV is substantially greater.

BTeV is competitive with LHCb in 'high-priority' final states with all charged particles. For final states with γ's, π^o's, η's or η''s, BTeV has a factor of $\approx$3.5 advantage. Furthermore, BTeV will write to tape a factor of 5 more b events than LHCb, allowing for more physics studies.

BTeV has all the components necessary to measure the most important quantities in heavy quark decays. These include spectacular vertex detection, triggering, particle identification, photon detection, and electron and muon identification. It is of crucial importance the decay time resolution in BTeV is about 45 fs, for most final states, which compares most favorably to the 900 fs in asymmetric e^+e^- colliders. The studies presented here were done on what is currently believed to be the most important modes. What's in fashion, however, changes. BTeV is a powerful enough detector to be able to test new and interesting ideas for all b species.

2.9 Appendix I: Update of Lepton Identification Techniques

In the proposal muon identification was taken from the muon detector alone and electron identification was ignored. In this update we now include muon and electron from the RICH detector and electron identification in the calorimeter.

Though it might seem that the mass difference between muons and pions is too small to provide useful separation using a Cherenkov based detector, because the Cherenkov angle goes as $(\cos\beta)^{-1}$, in fact there is significant separation over an interesting part of the momentum spectrum. More importantly, the RICH detector subtends a significantly larger solid angle than either the muon detector or the EM calorimeter.

Fig. 2.3 (left) shows the Cherenkov angle for different particle species as a function of momentum. The RICH angular resolution per track is expected to be 0.1 mr, as determined by a full simulation. In Fig. 2.3 (right) we have divided the difference in Cherenkov angles by the angular resolution.

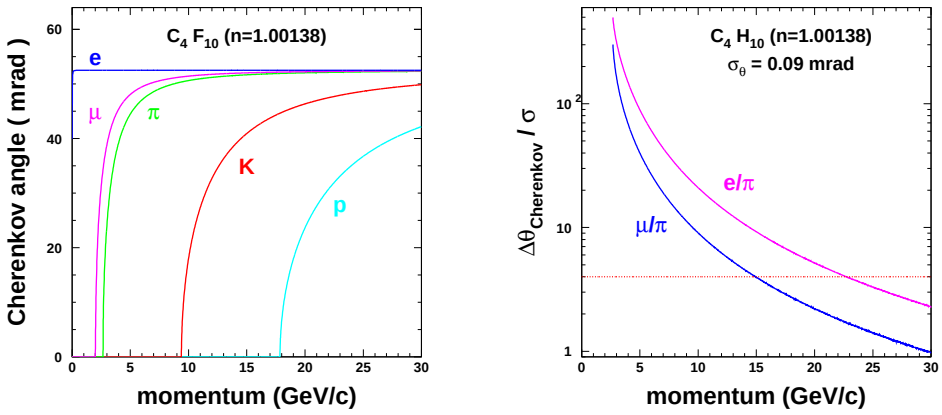

Figure 2.3: (left) The Cherenkov angle for the various particle species as a function of momentum. (right) The number of standard deviation separation for μ/π and e/π as a function of momentum. The dashed horizontal line is drawn at "4σ" separation.

To make a conservative estimate of the useful range of lepton identification from the RICH we require 4σ separation, i.e. the ratio of the difference in Cherenkov angles to the resolution be 4 or greater. For a 4σ separation requirement, the RICH detector can distinguish between muons and pions with momenta up to 15 GeV/c, and between electrons and pions up to 23 GeV/c.

To quantify our efficiency estimates we use the $B^o \to J/\psi K_s$, $J/\psi \to \ell^+\ell^-$ mode, because this is a bench mark mode. The J/ψ can be reconstructed both in the $\mu^+\mu^-$, and the e^+e^- modes. To illustrate the coverage of BTeV for lepton identification, we simulated only $\mu^+\mu^-$ mode; the e^+e^- mode is similar except for bremsstrallung, which we have ignored for now.

Figure 2.4 shows the polar angle distribution of the muons at the J/ψ decay vertex versus their momentum. Also shown are rough estimations of the angular coverage of the three detectors. Tracks at large angles, that are beyond detection in some systems, are at mostly lower energies. A significant number of high momentum tracks are not detected in the muon system because they have small angles. In this plot, each track passes a quality selection defined by requiring more than 20 hits, at least 4 of which must be in the pixel detector.

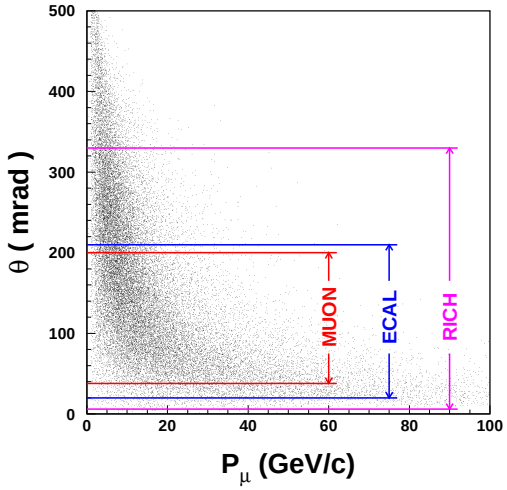

Figure 2.4: The momentum of muons from J/ψ decay versus their laboratory production angle. The lines indicate the geometric acceptance of the indicated detector elements in the absence of a magnetic field taking the origin as the center of the magnet (z=0).

For good tracks, the RICH detector has an acceptance of 95% for ±300 mr; the 5% loss results from magnetic field bending, the spread of the primary interaction position in z, and our requirement that the track be at least 10 cm within the aperture, a conservative requirement imposed to ensure that every track has a full Cherenkov ring. The ECAL detector has smaller angular coverage and the resulting acceptance is only about 66%.

The MUON detector also covers a smaller than ideal solid angle and has a relatively big hole around beam line. It also cannot detect tracks below 5 GeV/c The total acceptance is 48%. The missing tracks in MUON and ECAL are dominated by lower energy tracks at large polar angles. It is just these tracks that the RICH is capable of identifying.

We assume that the MUON detector has 100% identification efficiency within the acceptance. For ECAL, we use the efficiency curve as function of radius from $B^o \rightarrow K^*\gamma$ simulation (Figure 7.6 in the BTeV proposal). For RICH detector, we assume it has 100% efficiency in identifying muons between 2 GeV/c and 15 GeV/c, and electrons below 22.7 GeV/c. Although the RICH can still provide identification at somewhat higher momenta, for simplicity we just assume the efficiency is zero.

Different methods have been used to reconstruct $J/\psi \to \mu^+\mu^-$ in the proposal. One method is to simply identify both muons. This has an advantage of reducing backgrounds but can have low efficiency. (This method was used in the proposal for the $J/\psi K_s$ final state.) Another method is to require good muon identification for only one of the two muon tracks from a two-track detached vertex. (This method was used for the $J/\psi\eta^{(\prime)}$ studies.) Listed in Table 2.9 are J/ψ reconstruction efficiencies for different muon identification methods for the two J/ψ detection methods. Adding the RICH increases the efficiency by 19% when only one of two tracks is required to be a muon and a whopping 96% when both tracks are required to be identified. Using the RICH and MUON systems the difference between identifying one or two leptons is not as large, between 71% and 96%.

Table 2.9: Lepton identification efficiency for $J/\psi \to \mu^+\mu^-$.

	muon identification	
	single track	both tracks
MUON only	80.6 %	36.4%
MUON + RICH	96.0%	71.3%
Ratio	1.19	1.96

Although electron identification efficiency in ECAL is about 80% at large radii, the efficiency is much less at small radii where the density of tracks is high. The identification efficiency of $J/\psi \to e^+e^-$ is quite small using only ECAL identification as shown in Table 2.10. The RICH detector boosts the efficiency by 37% in the case where only one identified track is required. When both tracks are required to be identified, it boosts the efficiency by a factor of 3.

Table 2.10: Lepton identification efficiency for $J/\psi \to e^+e^-$.

	electron identification	
	single track	both tracks
ECAL only	69.3 %	21.6%
ECAL + RICH	94.9%	67.5%
Ratio	1.37	3.12

For lack of space in the hall the MUON detector is smaller than we like. For lack of money the ECAL is also smaller. However, the identification of muons and electrons is brought back to essentially full acceptance by use of the RICH. In summary, for dilepton final states, using both electrons and muons we increase the efficiency from the proposal by a factor of 2.4, for single lepton identification and 3.9 when positive identification of both leptons is insisted on.

2.10 Appendix II: Update on Flavor Tagging

2.10.1 Flavor Tagging Summary

Flavor tagging, determination of the flavor of the signal B hadron at the time of its production, is an essential component of the study of mixing and CP violation in B decays. It is also an area in which considerable sophistication is required. At the time of our proposal, we used a relatively simple approach. We have now completed a new study of the effective tagging power for B^o and B_s. These results, which will be discussed briefly here, supersede those presented in the May 2000 BTeV proposal. A complete discussion is available at *http://www-btev.fnal.gov/tagging.ps*.

We wish to optimize the flavor tagging "power", given by ϵD^2, where ϵ is the efficiency for obtaining a flavor tag and D is the dilution.

$$\epsilon = \frac{N_R + N_W}{\text{Total}}, \qquad D = \frac{(N_R - N_W)}{(N_R + N_W)}, \tag{2.1}$$

where N_R and N_W are the number of correct and incorrect tags, respectively, and "Total" refers to the sample of fully reconstructed neutral B mesons in the mode of interest.

The determination of the flavor tagging ϵD^2 takes advantage of the precision tracking provided by the pixel detector and excellent particle identification afforded by the RICH. We have studied the performance of the BTeV detector using four quasi-independent flavor-tagging methods. They are:

- Same Side Tagging (Kaon for B_s and Pion for B^o)
- Away Side Kaon Tagging
- Away Side Lepton Tagging
- Jet Charge Tag

Same Side Tagging algorithms utilize the correlation which emerges between a neutral B meson, called B_{CP} here, and the charge of nearby tracks produced in the fragmentation chain. Because these tracks are produced in the fragmentation of the b quark (not the decay), same side tag candidates emerge from the primary interaction vertex.

First let us discuss B_s tagging. When a B_s ($\overline{b}s$) forms, an extra $\overline{s}$ is available to form a K meson. About half of the time, it will produce a K^+ (the other half being K^0, which is not useful) which is 100% correlated with the flavor of the B_s at production. One nice feature of this tag is that it is not affected by the mixing of the tagging b, as in away side tagging.

For B^o mesons, the same analysis holds, except the particle tag is a charged pion. Unfortunately, there are a large number of charged pions from the interaction vertex, and hence the pion tag will have lower dilution than the kaon tag used for B_s. However, pion rates are somewhat enhanced because of the presence of B^{**} resonances. About $\sim$23% of B^o mesons

come from B^{**} [21], where the B^{**} decays into either a B^{*o} or B^o by emission of a single pion. Because of isospin, 2/3 of these are charged.

Away Side Tagging exploits the fact that in the strong interaction, b quarks are produced in pairs, and therefore the second (away side) b-quark in the event must have opposite flavor to B_{CP}. Therefore tagging the flavor of the away side b quark at production is a clean tag of the flavor of B_{CP}. Generally, this is done by examining the charge of kaons or leptons from the away side b-hadron decay or the charge of its associated jet. Since these particles come from the decay of the away side b hadron, away flavor tag algorithms usually exclude tracks which point back to the primary vertex. Because we examine the decay products, this method of flavor tagging is affected by mixing of the away side b. About 20% (50%) of B^o (B_s) mesons on the away side mix before decaying, and there are other factors that reduce the dilution. Away Side Kaon Tags exploit the fact that the away side b hadron usually undergoes the cascade $b \to c \to s$, of which half of these produce a K^-. Backgrounds which produce a K^+ include mixing, D_S decays, ϕ decays, etc. Despite these factors, the away side kaon tag has a very large dilution, as will be shown later.

Away Side Lepton tags are also useful. However, unlike the nearly 50% branching ratio for $\overline{B} \to K^- X$, the branching ratio of $b \to \ell^- X$ is about 10% each for electrons and muons. Lepton tags also have lower dilution than away side kaon tags because of the wrong sign leptons tags which arise from $b \to c \to \ell^+ X$. In the rest frame of the decaying b hadron, there is very nice kinematic separation between leptons from bottom and charm decays. However, without knowing the three momentum of the decaying b hadron, the separation is less effective. Nevertheless, leptons from b-hadron decay generally have significantly higher transverse momentum than those from charm, and this can be used to reduce the charm contamination. From the viewpoint of lepton production, electrons and muons should be nearly equally useful in flavor tagging. However, use of electrons for flavor tagging requires more sophistication in order to reject the large background from photon conversions (this problem clearly improves at large transverse momentum). We therefore will discuss in detail the away side muon tagging, and assume we can get about half the performance from the away side electron tags.

The idea behind the Jet Charge Tag is to reconstruct the location and decay products of the $b \to cW^-$ vertex. The particles associated with the W^- decay have a charge which is 100% correlated with the flavor of the parent b hadron. If we can reconstruct all the charged particles from the W decay, we would have a very clean flavor tag. As with other methods, the effectiveness of the jet charge tag is reduced, mainly by two factors. First, we do not reconstruct all the charged tracks from the W decay. Second, the charm decay vertex is often too close to the B decay vertex to separate the two vertices, resulting in a vertex that contains decay tracks from both the bottom and charm decay. Nevertheless, the jet charge algorithm does provide useful flavor tagging power. For all these tagging methods, except for jet charge and same side pion tags, excellent particle identification is required. Because there are ∼6-8 times as many pions as kaons in the momentum range of interest, excellent K/π separation is essential. Despite the proton/kaon ratio being less than one, substantial gains can be achieved with effective p/K separation.

2.10.2 Simulation and Event Selection

Two event samples are used in this analysis, both generated Pythia. For B_s, a sample of $B_s \to J/\psi K^{*0} \to \mu^+\mu^- K^+\pi^-$ events were generated. For B^o, a sample of $B^o \to J/\psi K^0_S \to \mu^+\mu^-\pi^+\pi^-$ were generated. For the latter sample, we modified the default Pythia parameters in order to produce B^{**}'s which are not normally produced [22]. For both B_s and B^o, we include the effects of mixing. Long-lived particles were decayed using the QQ package [23]. The events were then passed through the *mcfast* detector simulation with a geometry that describes the BTeV detector components. The detector simulation includes the effects of secondary interactions, multiple scattering, conversions, decays in flight and energy loss in material.

Events which had a fully reconstructed B_{CP} (B_s or B^o) hadron were passed on to the flavor tagging analysis. To be considered for a kaon or lepton tag, tracks were required to have at least 4 pixel hits and at least three three-dimensional hits in the downstream tracking chambers. In addition, tracks were required to be within the acceptance of the RICH. To be considered for the same side tag analysis, a track was required to have D/ $\sigma < 3$ [24]. For the away side analysis, kaon candidate tracks were required to have D/σ >3, but muon candidates were not subject to this requirement.

2.10.3 B_s Flavor Tagging

Here, we discuss in some detail the B_s analysis, using all four tagging methods described above. Later, we give a briefer description of the B^o analysis which focuses on the differences with the B_s analysis.

2.10.3.1 Same Side Kaon Tag

One important task is to make sure that the tagging particle is indeed a kaon. The C_4F_{10} gas radiator section of the RICH has outstanding K/π discrimination over this momentum range so pion contamination is negligible. To discriminate against proton background, we use both the liquid and gas radiator sections of the RICH and require that

1. The track is in acceptance of the RICH system.
2. If p $\leq$ 3 GeV/c, the track must be inside the active area of the liquid radiator.
3. If p $\leq$ 9.5 GeV/c and the candidate is in the liquid radiator acceptance, there must be at least two reconstructed photons for the kaon hypothesis from the liquid radiator.
4. If 9.5 $<$ p $\leq$ 10.5 GeV/c, the kaon hypothesis must have a non-zero likelihood determined by the gas system.
5. For p $>$ 10.5 GeV/c, there must be at least 5 reconstructed photons from the gas radiator for the kaon hypothesis.

We use the particle ID likelihoods to form signal and background distributions of $\Delta\chi^2 = -2 \times log(L_{pr}/L_{ka})$, where L_{pr} and L_{ka} are the likelihoods for the proton and kaon hypotheses respectively.

There are several sources of background kaons that cause errors in determining the flavor. We have found three relatively uncorrelated kinematic variables which have some power to discriminate the fragmentation kaons we want to use from other sources of kaons. These variables are:

- $\Delta\phi$, the difference in azimuthal angle between the reconstructed B_s and the kaon candidate,
- $\Delta\eta$, the difference in pseudorapidity between the B_s and the kaon candidate, and
- Q, the difference in invariant mass between the B_s + kaon candidate and the B_s itself.

Since each event may contain multiple kaon candidates, we need a method by which to determine an "event charge" associated with the same side kaon, which in turn determines the flavor of the B_s. This is done in the following manner. For each kaon candidate in an event, we calculate the signal probability (P_{sig}) and background probability (P_{bak}), determined from Monte Carlo. Each of these is given by a product of probabilities from the signal and background distributions in $\Delta\phi$, $\Delta\eta$, Q and $\Delta\chi^2$. We then define a discriminant, X_{tag} given by:

$$X_{tag} = \frac{1 - \prod_{i=1}^{4}(P^i_{sig}/P^i_{bak})}{1 + \prod_{i=1}^{4}(P^i_{sig}/P^i_{bak})}$$

The index i runs over the four input variables. By definition, $-1 \leq X_{tag} \leq 1$. Signal kaons peak at low values of X_{tag} and background kaons tend to be flat or peak toward positive values of X_{tag}. We select kaon candidates with $X_{tag} < X_{cut}$, where X_{cut} is between -1 and 1. In Fig. 2.5 we show the distribution in X_{tag}. A clear peak toward negative values for signal kaons is evident, and the background is nearly flat. The spike at $X_{tag} = 1$ consists of protons which have low probability for being a kaon.

For a given cut on X_{tag}, we divide the sample into events in which the event weighted charge gives the correct B_s flavor (N_R), and the incorrect flavor (N_W). We compute the efficiency as the sum of N_R+N_W divided by the total reconstructed B_s sample and dilution according to equation 2.1. We find that the maximum tagging power is obtained for a cut on $X_{tag} < -0.2$ for which $\epsilon D^2 = 5.7\%$, with a corresponding efficiency of 36% and a dilution of 40%.

2.10.3.2 Away Side Kaon Tagging

As discussed above, Away Side Kaon Tags rely on detecting the kaon associated with the $b \to c \to s$ cascade which produces a charged kaon about half the time. Because the away side kaon tag is a high purity sample for flavor tagging, proton contamination must be minimized using the RICH information. The tagging method follows much of the same formalism as

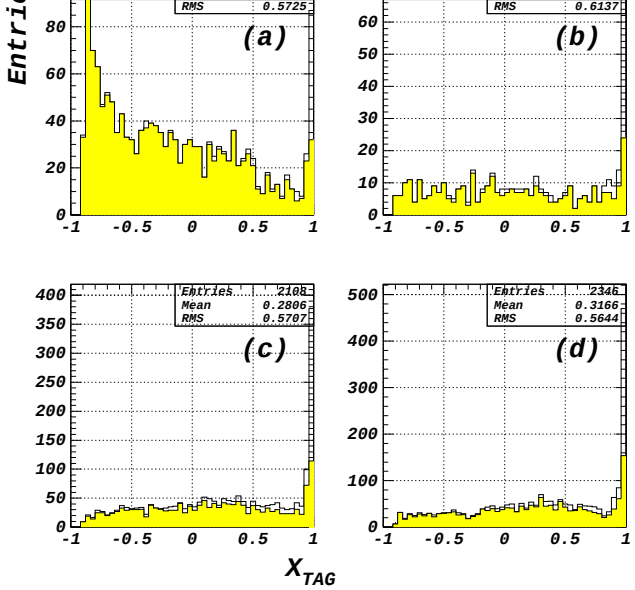

Figure 2.5: The distribution in X_{tag} for a) kaons which correctly determine the B_s flavor and are part of the B_s fragmentation, (b) kaons which incorrectly determine the B_s flavor and are part of the B_s fragmentation, (c) kaons which correctly determine the B_s flavor but are not part of the B_s fragmentation, (b) kaons which incorrectly determine the B_s flavor and are not part of the B_s fragmentation. The unfilled histogram shows the distribution for all kaon candidates and the shaded histogram shows the distribution for true kaons.

the same side kaon tag analysis, except that the track is required to have $D/\sigma > 3$. We also require that the impact parameter to the primary vertex is less than 2 mm which is $\sim$97% efficient for particles from b-hadron decay. Furthermore, we use only the $\Delta\phi$ and $\Delta\chi^2$ information in our discriminant, since there is little or no correlation in $\Delta\eta$ and Q of the away side kaon candidate with the reconstructed B_s.

Kaons which give the wrong flavor tag are mostly due to B mixing, D_s, and ϕ decays. The wrong sign kaons are about 25% of the right sign. This source of tagging dilution is unavoidable, since it is from genuine B decays. There is also a contamination from protons, which is significant because of the non-negligible rate for $B \to p/\overline{p}$ ($\sim$8%). The particle identification information from the RICH can eliminate the false tags due to protons.

Using the same procedure as described for the same side tags, we form an event charge, and categorize events according to whether the event charge gives the correct or the incorrect flavor for the B_s. As expected, we do not gain much by making a tight requirement on X_{tag} since the background is largely from wrong sign kaons from B decays which have a similar shape in X_{tag} to right sign kaons. However, some events have multiple kaon candidates, so the charge weighting procedure is useful. We achieve an $\epsilon D^2 = 5.8\%$, corresponding to $\epsilon \sim 16.5\%$ and $D \sim 59\%$.

2.10.3.3 Away Side Muon Tagging

The Away Side Muon Tagging follows the same procedure as the away side kaon tagging, except we remove the requirement that the muon have $D/\sigma < 3$, since we expect the prompt muon background in events with a reconstructed b hadron to be small. We assume perfect muon identification using the RICH and muon systems. Decays in flight are modeled in

our simulation, but they generally have much larger impact parameter than muons from B decay, and hence do not have pixel and/or downstream tracks. For muon tags, the correct flavor tag is mainly from the $\overline{B} \to \mu^- X$ decay. A small fraction of right sign tags come from $D \to \mu^- X$ where the B^o has mixed. B mixing and leptons from the semileptonic decay of charm constitute the main source of wrong sign muons. Because of the latter, we expect the dilution to be worse for away side muon tags than away side kaon tags. In addition, the branching fraction for $B \to \mu^{\pm} X$ (including $b \to c \to \mu X$) is about 40% of $B \to K^{\pm} X$.

The right sign muons, from $B \to \mu X$, have a much stiffer P_T distribution than do the wrong sign, predominantly from $D \to \mu X$. In this analysis, there is a cut on the transverse momentum of the muon at 0.4 GeV/c to reduce the $D \to \mu X$ background . We also find that the acceptance for B muons (∼60%) is larger than D muons (∼37%), mainly due to the stiffer momentum spectrum for B muons. Non-b decay related backgrounds are negligible.

Just as with the away side kaon tags, an event charge is computed, although only 3% of the events have two reconstructed muons. However, one observes that since most wrong sign muons are from a B-related charm daughter, the maximum value of the tagging power is achieved by not making any cut on X_{tag}. Therefore, the results are essentially identical to having simply counted the number of right sign and wrong sign muons. With no requirement on X_{tag} we obtain an efficiency, $\epsilon = 8\%$, a dilution $D = 40\%$, and $\epsilon D^2 = 1.3\%$.

We have not carried out the more complicated study of Away Side Lepton Tagging using electrons/positrons, but plan to do so soon.

2.10.3.4 Jet Charge Tagging

Jet charge tagging has been successfully used in hadron collider experiments [25]. The philosophy behind the jet charge is to reconstruct the tracks associated with the W decay in $b \to W^{\pm} c$ for the away side b hadron. The total charge of the tracks associated with the W give the flavor of the decaying b hadron, and hence of B_{CP}.

First, we utilize only charged tracks with $D/\sigma > 3$ and $D < 5$ mm (i.e., "secondary tracks") to search for displaced (or secondary) vertices. Because of the high purity of secondary kaons and muons, they are only required to have a $P_T > 0.1$ GeV/c, whereas all other particles are required to have $P_T > 0.2$ GeV/c. The procedure loops over all track pairs, and fits them to a common vertex. If the χ^2 probability is greater than 1%, the vertex is kept. The algorithm then attempts to attach other tracks which have $D/\sigma < 2.5$ with respect to the candidate decay vertex. If the addition of the track results in a $\chi^2/dof < 2.5$ for the vertex fit, the track list for the vertex is updated and the new vertex parameters stored. The process continues until all track pairs have been used as "seed tracks" for a vertex. This is done to avoid order dependence of the vertexing. As new vertices are formed, they are compared to the existing ones, and duplicates are removed. If no vertex is found, we take the highest P_T secondary track, as long as $P_T > 1$ GeV/c. For each secondary vertex, we compute the jet charge (JETQ), defined as:

$$JETQ = \frac{\sum r_i(P_T)(p_i \cdot \hat{n})^k \times Q_i}{\sum r_i(P_T)(p_i \cdot \hat{n})^k}$$

The weights, $r_i(P_T)$ are functions of P_T and give the relative probabilities for π, K, P, e, and μ to give the correct flavor of the parent B. Usage of this factor is enabled by the excellent particle identification provided by the RICH. In determining the weights, we flip the charge of all protons, as their charge is anti-correlated with the b flavor [26], and flip the charge of electrons and muons with $P_T < 0.8$ GeV/c, since it is more probable that these are from charm decay, in which case the charge is anti-correlated.

The term $p_i \cdot \hat{n}$ gives the component of the track's momentum (p_i) along the axis of the jet ($\hat{n}$), and k is an exponent which is generally varied between 0 and 1 to optimize the performance of the jet charge tag. The "jet" axis is defined using the tracks in the secondary vertex. We compared three values for the exponent, 0, 0.5, and 1.0, and we find that the highest flavor tagging efficiency is obtained for $k = 0$. Given a list of vertices, we choose the one with the highest track multiplicity as this gives the largest dilution [27]. In Fig. 2.6, we compare the tagging power as a function of the number of tracks in the vertex for the $k = 0$ case. In this case, the correct charge corresponds to JETQ = -1. For the case where only a single track was found, we reject events in which the track is a $\pi^{\pm}$ because it is ineffective (i.e., $D \sim 0$). Also, to improve the dilution for 3 track vertices, we have required $|JETQ| > 0.2$. While the jet charge tag is highly correlated with the away side kaon and away side muon tags, as a stand-alone tagger, we achieve $\epsilon D^2 = 4.5\%$, with a corresponding efficiency of about 33% and a dilution of ∼37%.

2.10.4 B^o Flavor Tagging

Flavor tagging for the B^o uses the same techniques as B_s for away side kaon tagging, away side muon tagging and jet charge tagging. These results compare well with those derived from the independent sample of B_s events. Same Side Tagging is less effective for B^o than for B_s.

2.10.4.1 Same Side Pion tagging

For the same side tag, we search for charged pions which are consistent with being from the fragmentation of the b-quark. As mentioned above, we tune the MC to produce the correct rate of B^{**} relative to B [21]. If the correct $\pi^{\pm}$ is reconstructed and selected, such combinations produce a pronounced peak in the $Q = M(B^o+\pi) - M(B^o) - M(\pi)$ distribution at about 300 MeV. Since these pions point back to the interaction vertex, there is a very large pion background. We find that the $\Delta\eta$ distribution degrades the results for ϵD^2, so we do not use this in computing signal and background probabilities. Otherwise, we use the same procedure as was done for same side kaon tags. For the same side pion tag, we find and $\epsilon D^2 = 1.8\%$, which corresponds to an efficiency of 90% and a dilution of 14%.

2.10.4.2 Away Side Kaon and Muon Tagging and Jet Charge Tagging

The analysis of the Away Side Kaon tagging for B^o is exactly the same as for B_s. Following the same procedure, we find $\epsilon D^2 = 6.0\%$ with an efficiency of 19% and a dilution of 57%. For

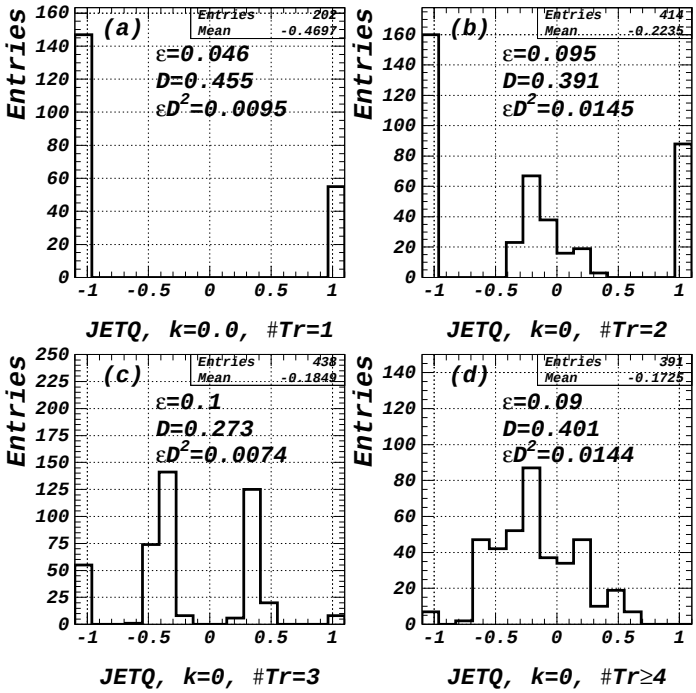

Figure 2.6: The distribution of jet charge for different number of tracks, using $k = 0.0$ as described in the text: (a) single track (b) 2 track vertices, (c) 3 track vertices, and (d) 4 or more track vertices. Also shown in each figure are the efficiencies, dilutions and tagging power values.

Away Side Muon Tagging, using the same procedure as was done for B_s, we find $\epsilon D^2 = 1.2\%$. Finally, for Jet Charge Tagging we find $\epsilon D^2 = 4.8\%$.

2.10.5 Combining Flavor Tags

We have used a simple approach to combining the tagging algorithms. We simply rank the algorithms in order of decreasing dilution, and the algorithm highest on the list determines the flavor tag for a given event. If an event is not tagged by the first algorithm, we check the second, and so on. In this way, the flavor determination comes from a single tag algorithm, the one with the highest dilution. For B_s, the hierarchy is: away side kaon tag, away side muon tag, same side kaon tag, and jet charge tag. For B^o, the jet charge has higher dilution than the same side pion tag, so the order is reversed.

2.10.6 Final Results

The final results for ϵD^2 for B_s are shown in Table. 2.11 and for B^o in Table 2.12. The second column shows the results if the taggers are treated independently, and the third

column shows the results when overlaps are removed. For B_S, the high degree of correlation between the away-side tags and the jet charge tag is evident, as only 1/3 of the events tagged by jet charge are not tagged by one of the three other algorithms. Also, the average dilution of the jet charge drops to 37%, when all events are used, to 20%, when overlaps are removed. We have not yet performed a sophisticated likelihood analysis in which the correlations are used to improve the combined ϵD^2. Also, note that the away-side electron tags are not explicitly treated, and we might expect to get another 0.7% in ϵD^2. Therefore, we expect to achieve an ϵD^2 of 13% for B_s decays and 10% for B^o decays.

Table 2.11: Results on ϵD^2 for the four tagging algorithms for B_s. Shown are the results of the individual taggers, and the results when overlaps are removed.

Sample	Independent Tag $\epsilon D^2(\%)$	Overlaps removed $\epsilon D^2(\%)$
Away side Kaon Tag	5.8	5.8
Away side Muon Tag	1.3	1.3
Same side Kaon Tag	5.7	4.5
Jet Charge Tag	4.5	0.4
Sum	-	12.1
Electrons + Likelihood Fit	-	0.9
BTeV Expected		13

Table 2.12: Results on ϵD^2 for the four tagging algorithms for B^o. Shown are the results of the individual taggers, and the results when overlaps are removed.

Sample	Independent Tag $\epsilon D^2(\%)$	Overlaps removed $\epsilon D^2(\%)$
Away side Kaon Tag	6.0	6.0
Away side Muon Tag	1.2	0.8
Jet Charge Tag	4.8	1.4
Same side Pion Tag	1.8	1.0
Sum	-	9.2
Electrons + Likelihood Fit	-	0.8
BTeV Expected		10

Bibliography

[1] A. E. Snyder and H. R. Quinn, *Phys. Rev. D* **48** (1993) 2139.

[2] H. R. Quinn and J. P. Silva, "The Use of Early Data on $B \to \rho\pi$ Decays," hep-ph/0001290 (2000).

[3] K. Abe *et al*, *Phys. Rev. Lett.* **88**, 021801 (2002) (hep-ex/0109026).

[4] See *B Decays, revised 2nd Edition* ed. S. Stone, World Scientific, Singapore, (1994).

[5] B. Aubert *et al*, *Phys. Rev. Lett.* **87**, 091801 (2001), *ibid.* **86**, 2525 (2001), and B. Aubert *et al*, "A Study of Time-Dependent CP-Violating Asymmetries and Flavor Oscillations in Neutral B Decays at the Upsilon(4S)," (hep-ex/0201020) (2002); K. Abe etal, *Phys. Rev. Lett.* **87**, 091802 (2001).

[6] B. Aubert *et al* (BABAR), "Study of CP-violating asymmetries in $B^o \to \pi^+\pi^-$, $K^+\pi^-$ decays," (hep-ex/0110062) (2001).

[7] Z. Zhao *et al*, "Report of Snowmass 2001 Working Group E2: Electron-positron Colliders from the ϕ to the Z," to appear in the proceedings (hep-ex/0201047).

[8] S. Henderson, "M2: Summary -Electron-Positron Circular Colliders," presented at Snowmass 2001, to appear in the proceedings, http://vmsstreamer1.fnal.gov/VMS_Site_02/Lectures/Snowmass2001/720M2Henderson/sld016.htm

[9] DOE/NSF HIGH-ENERGY PHYSICS ADVISORY PANEL SUBPANEL ON LONG RANGE PLANNING FOR U.S. HIGH-ENERGY PHYSICS, available at http://doe-hep.hep.net/.

[10] P. Ball *et al*, "B decays at the LHC," CERN-TH/2000-101 (hep-ph-0003238).

[11] K. Abe *et al.*, (CDF), *Phys. Rev. Lett.* **75**, 1451 (1995); S. Abachi *et al.*, (D0), *Phys. Rev. Lett.* **74**, 3548 (1995). See also the UA1 measurement C. Albajar *et al.*, *Phys. Lett.* B**186**, 237 (1987); B**213**, 405 (1988); B**256**, 121 (1991).

[12] K. Abe *et al.*, (CDF), *Phys. Rev. Lett.* **76**, 4462 (1996); ibid **77**, 1945 (1996); K. Abe *et al.*, (CDF), *Phys. Rev. D* **57**, 5382 (1998).

[13] T. Junk, "A Review of B Hadron Lifetime Measurements from LEP, the Tevatron and SLC," in Proceedings of the 2nd Int. Conf. on *B Physics and CP Violation*, Univ. of Hawaii, (1997), ed. T. E. Browder *et al.*, World Scientific, Singapore (1998).

[14] K. Abe *et al.*, (CDF), "Observation of B_c Mesons in $p-\overline{p}$ Collisions at $\sqrt{s} = 1.8$ TeV," hep-ex/9804014 (1998).

[15] M. Paulini, "B Lifetimes, Mixing and CP Violation at CDF," Review article to appear in the Int. Journal of Modern Physics A, hep-ex/9903002 (1999).

[16] K. Anikeev *et al*, "B Physis at the Tevatron: Run II and Beyond, "FERMILAB-PUB-01/197 (hep-ph/0201071) (2001).

[17] "LHCb Technical Proposal," CERN/LHCC 98-4, LHCC/P4 (1998), available at http://lhcb.cern.ch .

[18] We have confirmed with T. Nakada, the LHCb spokesperson, that the yields for this mode as quoted in their Technical Proposal are their current values that we should use in our comparisons. The branching ratio numbers used by LHCb were taken from Table 15.11 on page 157. The number of events were taken from Table 15.12. Since these numbers are quoted as being "tagged," we divided by the 0.40 tagging efficiency given on page 145. The two final states $\rho^+\pi^-$ and $\rho^-\pi^+$ are given separately by LHCb; we added them together. The same procedure was followed for $B_s \to D_s K$.

[19] P. Ball *et al.*, "B Decays at the LHC," CERN-TH/2000-101, hep-ph/0003238.

[20] Although they state a 1% efficiency here, this is only a partial efficiency according to T. Nakada.

[21] T. Affolder *et al.*, (CDF), *Phys. Rev. D.* **64**, 072002 (2001); N. Harnew, P.E. Schlein, BEAUTY 95, Proceedings of the Third International Workshop on B Physics at Hadron Machines, University of Oxford, UK, July 10-14, 1995; R. Akers *et al.*, (OPAL Collaboration) *Z. Phys. C.* **66**, 19 (1995).

[22] The parameters PARJ(14) - PARJ(17) were change from 0.0 to 0.05, which allows for the production of higher spin and angular momentum states.

[23] For a description of the QQ generator see http://www.lns.cornell.edu/public/CLEO/soft/QQ (unpublished).

[24] The quantity D/σ is the distance of closest approach of the track to the primary vertex divided by the uncertainty in that distance.

[25] T. Affolder *et al.*, (CDF), *Phys. Rev. D.* **60**, 072003 (1999).

[26] Protons from b decay frequently come from $b \to \Lambda_b \to \Lambda_c + X$, with $\Lambda_c \to p + X$. So the positively charged proton is correlated with the negatively charged b quark, and visa versa.

[27] Strictly speaking, the single-track sample has a larger dilution, but we expect these are only used when there are no multi-track vertices in the event. Also, we expect that many of the single-track candidates will be accounted for in the away side tag analyses.